Waste and Biomass Valorization (2022) 13:2411–2423
https://doi.org/10.1007/s12649-021-01658-w

ORIGINAL PAPER

Artemisia annua Stems a New Sustainable Source for Cellulosic Materials: Production and Characterization of Cellulose Microfibers and Nanocrystals

Heriarivelo Risite[1] · Mohamed Hamid Salim[2] · Bricharles T. Oudinot[1] · El-houssaine Ablouh[2] · Heriniaina T. Joyeux[1] · Houssine Sehaqui[2] · Jean Hugues A. Razafimahatratra[3] · Abou El Kacem Qaiss[4] · Mounir El Achaby[2] · Zineb Kassab[2]

Received: 29 April 2021 / Accepted: 2 December 2021 / Published online: 23 January 2022

Abstract

In this study, *Artemisia annua* stem waste was identified, for the first time, as a potential natural source to produce cellulose microfibers (CMF), as well as cellulose nanocrystals (CNC) with unique functionalities by using various organic acids. The CMF extraction was carried out using alkali and bleaching treatments, while the CNC were isolated under acid hydrolysis by using sulfuric acid (S-CNC), phosphoric acid (P-CNC), and hydrochloric acid / citric acid mixture (C-CNC). The CMF and CNC physicochemical, structural, morphological, dimensional, and thermal properties were characterized. CMF with a yield of 53%, diameter of 5 to 30 µm and crystallinity of 57% were successfully obtained. In contrast, CNC showed a rod-like shape with an aspect ratio of 53, 95, and 64 and a crystallinity index of 84, 79, and 72% for S-CNC, P-CNC, and C-CNC, respectively. Results suggested that the type of acid significantly influenced the structure, morphology, and thermal stability of CNCs. Based on these results, *Artemisia annua* stem waste is a great candidate source for cellulose derivatives with excellent characteristics.

✉ Mounir El Achaby
mounir.elachaby@um6p.ma

✉ Zineb Kassab
zineb.kassab@um6p.ma

[1] Laboratoire de Physique et Environnement, Université de Toliara, 601 Toliara, Madagascar

[2] Materials Science, Energy and Nano-Engineering Department (MSN), Mohammed VI Polytechnic University (UM6P), Lot 660 – Hay Moulay Rachid, 43150 Ben Guerir, Morocco

[3] Laboratoire de Chimie organique, Université de Toliara, 601 Toliara, Madagascar

[4] Composites and Nanocomposites Center (CNC), Moroccan Foundation for Advanced Science, Innovation and Research (MAScIR), Rabat Design Center, Rue Mohamed El Jazouli, Madinat El Irfane, 10100 Rabat, Morocco

Graphical Abstract

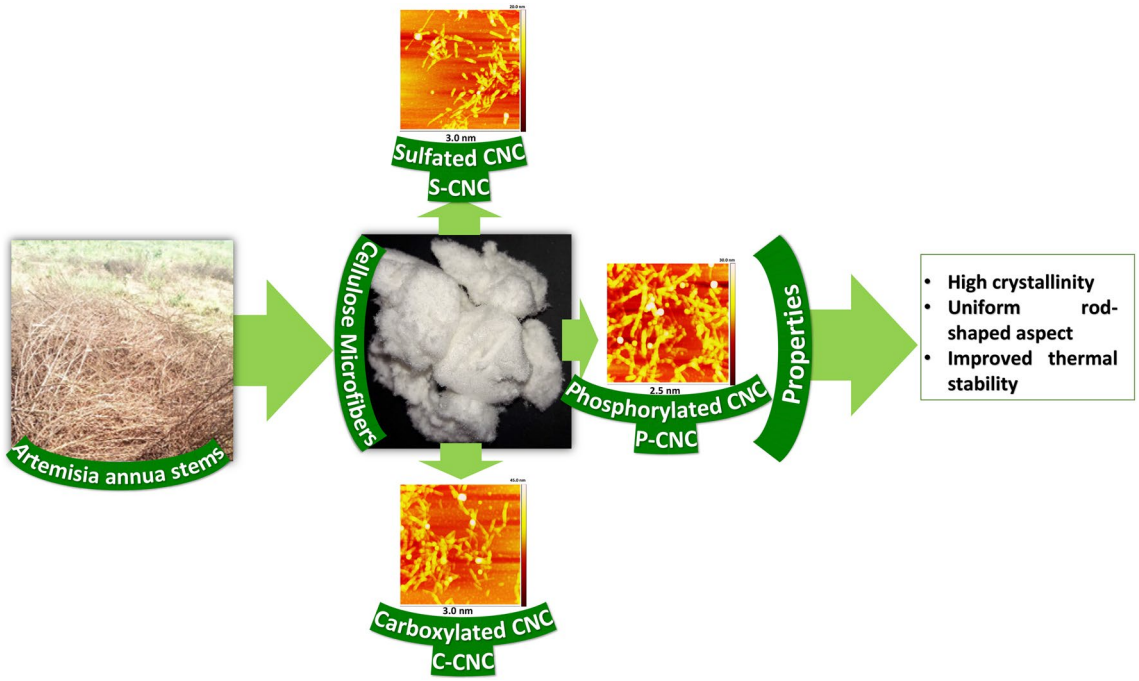

Keywords Cellulose microfibers · Cellulose nanocrystals · *Artemisia annua* · Renewable resource

Statement of Novelty

Different industries such as the pharmaceutical and agri-food sectors produce huge amounts of renewable agricultural waste, which could be considered a good cellulose source. Upgrading biomass into valuable products is the best way to overcome these limitations. Therefore, this paper presents novel research on using *Artemisia annua* stem waste, a new non-conventional unexplored cellulose resource, to isolate cellulose microfibers (CMF) via alkali and bleaching treatments and cellulose nanocrystals (CNC) with unique properties using different acid hydrolysis. The effects of the hydrolysis using sulfuric, phosphoric, and citric/hydrochloric acids on the morphology, structure, and properties of the resultant CNC were investigated. The methods provided here are a very versatile and simple procedure for preparing CNC that is thought to be a better alternative to the generally used, extensive, multistep, and time-consuming post-functionalization processes.

Introduction

Cellulose, the most widely available renewable biomacromolecule available on the earth, and is widely used because of its biodegradability, biocompatibility, and chemical stability [1–5]. The major source of cellulose is wood [6–8]. However, with the increasing consumption of wood resources, deforestation and global climate change have steadily increased interest in agricultural products and by-products as an alternative source of cellulose [6, 9, 10]. Agricultural waste is the most abundant green renewable and sustainable resource residue on earth [10–12]. In this sense, these sources constitute an excellent alternative to produce novel value-added materials that represent an economic advantage for industries such as the food and packaging sectors, guided by the prominence of ecology and green chemistry [13–16]. However, its exploitation constitutes an essential solution for agricultural biomass. In recent years, these bio-based sources have attracted immense research interest to develop a new approach that can add a high value to these residues by joining novel material functions and minimizing the impact on the environment [10, 14, 17, 18]. Among this biomass, it can be mentioned spruce bark, tomato plant residue, sago seed shells, acacia bark, tea leaf, garlic straw residue, and corn stover, which are the aim of several studies on the extraction of cellulosic micro and nanomaterials that hold promise in many different applications such as packaging, biomedical, energy storage, catalysis, etc. [1–5, 13, 19–21]. However, there are still several types of biomass that have not yet been exploited in this way, such as *Artemisia annua* (*Artemisia annua* L.) stem waste, which the plant

has long been grown and used in herbal medicine as early as 168 BC, particularly in ancient China [22], and also it has been used as a source of anti-malarial drugs [23, 24]. Researchers are currently investigating its use in COVID-19 treatment and, more broadly, as a medication for respiratory infections [25, 26].

Artemisia annua plant is also grown in several other countries such as Madagascar, India, Thailand, Australia, Brazil, Switzerland, Netherlands, and France [23]. Moreover, it is reported that the plant is adaptable to various types of soil [27]. The worldwide dry weight of the *Artemisia annua* plant harvest ranges from 2 to 6.8 t/ha in a field where the annual planting density varies from 1 to 20 plants/m^2 [28]. The plant is best harvested in the budding flower state, where the whole plant is harvested and cut into branches, left to dry either in the sun or else in an oven, and the dry branches are shaken or pounded to remove the leaves from the stem [29]. The leaves are then transferred for further processing, mostly to the pharmaceutical industries, while the stems are dumped as waste [29]. Hence, the exploitation of *Artemisia annua* plants to extract bioactive molecules will generate stem waste rich in lignocellulosic fibers, which can be used as an essential bio-based source for the extraction of cellulosic materials and their derivatives. Additionally, the global cellulose production from all resources is expected to rise significantly, from $250 million in 2019 to $783 million in 2025 [1, 30]. Hence, the current work adds value to *Artemisia annua* stem residues as a source of cellulosic materials.

Many processes can be applied to remove compounds surrounding the pure cellulose to extract cellulose fibers from biomass sources [8, 16, 31]. Researchers used chemical methods such as alkalization and bleaching treatments [8]. The role of the two treatments above is the removal of non-cellulosic components presented in the raw matter, namely lignin, hemicellulose, and other extractive substances, leading to the production of purified cellulose microfibers (CMF) [8, 32]. CMF consists of a mixture of amorphous and crystalline regions and exhibits a fiber diameter generally of several micrometers [6, 33].

The use of acid hydrolysis process to breakdown the purified cellulose fibers is the most widely applied technique, where the cellulose fibers are subjected to concentrated acid to remove the amorphous domains of the cellulose chains and leaving the crystalline domains unaltered, named cellulose nanocrystals (CNC) [1, 6, 9]. Hydrolysis conditions such as temperature, reaction time, the concentration used, and type of acid; need to be controlled during the acid hydrolysis process because the change of these factors directly affects CNC characteristics [6]. In the hydrolysis process, various forms of inorganic acids can be used, including sulfuric acid (H_2SO_4) [9], phosphoric acid (H_3PO_4) [1], a mixture of citric acid ($C_6H_8O_7$), and hydrochloric acid (HCl) [1]. The hydrolysis by sulfuric acid attaches anionic sulfate groups to the cellulose surface, while phosphoric acid generates phosphate groups [1, 6]. Hydrochloric acid hydrolysis produces hydroxyl groups on the surface, whereas hydrolysis using the mixture of hydrochloric acid and citric acid was reported to result in carboxylate functionalized CNC [1]. These CNC have attracted huge interest as a novel nanomaterial due to its excellent mechanical properties in nanocomposite materials [33–35].

To the best of our knowledge, the isolation of pure CMF and CNC from Artemisia annua stems have not been reported in the literature. Thus, this study aims to exploit the available and unexploited *Artemisia annua* stem waste as a bio-resource to produce CMF and CNC with different surface functionalities. The use of sulfuric acid, phosphoric acid, and citric/hydrochloric mixture acid hydrolysis processes resulted in the isolation of sulfated CNC (S-CNC), phosphorylated CNC (P-CNC), and carboxylated CNC (C-CNC), respectively. Furthermore, the obtained CMF and CNC (S-CNC, P-CNC, and C-CNC) properties were studied in terms of their morphology, structure, crystallinity, size, and thermal stability.

Experimental Details

Materials

Raw Artemisia annua stem waste (R-AS) as cellulosic raw material for extracting CMF and CNC were obtained from Madagascar. The raw plant was first dried, the dry leaves were removed, and the stems were collected and crushed. All used chemicals such as sulfuric acid (95–97%), hydrochloric acid (37%), phosphoric acid (85%), sodium hydroxide, citric acid (99.5%), acetic acid (99%), and sodium chlorite (80%) were obtained from Sigma Aldrich.

Cellulose Microfibers (CMF) Isolation

The extraction of CMF from stem waste of the *Artemisia annua* plant was directed through successive isolation of hemicelluloses, lignin, and other non-cellulosic components such as proteins, waxes, and fats via washing, alkaline, and bleaching treatments as often reported in previous works [6, 33]. 10 g of raw *Artemisia annua* stem waste (R-AS) were first treated with distilled hot water, followed by an alkaline treatment using NaOH (4 wt.%) at 80 °C for 2 h to obtain 6.5 g of alkali-treated *Artemisia annua* fibers (AT-AS) (Fig. 1), which is equivalent to 65% yield of initial R-AS. Afterward, to produce CMF, the alkali-treated fibers were treated 3 times using a solution made up of equal parts (v:v) of acetate buffer (75 mL glacial acetic acid/27 g of sodium hydroxide/1 L of distilled water) and aqueous $NaClO_2$ in

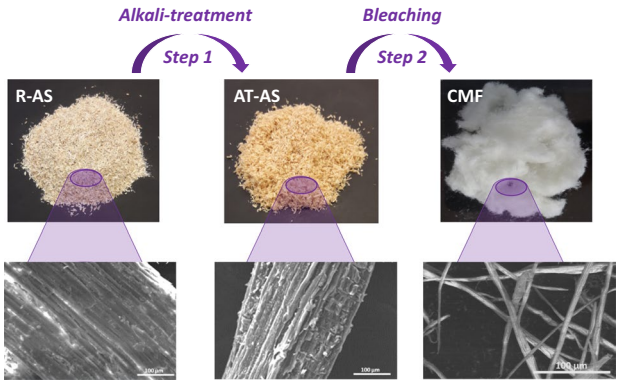

Fig. 1 Digital images of raw Artemisia annua stem waste (R-AS), alkali-treated fibers (AT-AS), cellulose microfibers (CMF) on top, and their corresponding SEM images below

water (1.7 wt%). The fibers/liquid ratio was 1/20 (g/mL). After washing and drying, 5.3 g white-colored fibers (53% yield regarding the initial mass of R-AS) were obtained and named CMF (Fig. 1).

Preparation of Cellulose Nanocrystals (S-CNC, P-CNC, and C-CNC)

Three types of CNC were obtained from CMF fibers by using sulfuric, phosphoric, and a mixture of hydrochloric/citric acid hydrolysis. As demonstrated in Fig. 2, CNC suspensions were obtained after acid hydrolysis and left to cool at ambient temperature. The suspensions were then repeatedly washed using distilled water by multiple rinsing and centrifugation steps until reached a neutral pH. The suspensions were further probe sonicated continuously for 15 min in an ice bath. Finally, the obtained suspensions were transformed into a dried form using the freeze-drying process (Fig. 2). The yield of obtained CNC was 18%, 28%, and 26% for S-CNC, P-CNC, and C-CNC, respectively, compared to the initial R-AS.

Characterization Techniques

The chemical composition of the Artemisia stem waste was done using TAPPI (Technical Association of the Pulp and Paper Associations) standard methods. Firstly, the sample was prepared according to the standard TAPPI T 210 cm-03 method. The composition of the raw fibers was determined according to the following methods: cellulose and hemicellulose (TAPPI T 203 cm-99), acid-insoluble lignin (TAPPI T 222 om-02), moisture (TAPPI T 550 om-99), and ash (TAPPI T 211 om-02). On the other hand, the holocellulose content was determined according to Wise et al. method [36]. FTIR spectroscopy analysis was carried out using FTIR, Perkin-Elmer Spectrum 2000 equipped with an ATR accessory. The FTIR spectra were taken in the transmittance mode in the range of 4000–600 cm^{-1} with a resolution of 4 cm^{-1} and an accumulation of 16 scans. X-ray diffraction (XRD) characterization was performed using a D2 PHASER diffractometer BRUKER using copper radiation ($\lambda = 1.54056$ Å) in the 2θ range of 5–50° with a step size of 2° at room temperature. The crystallinity index (*CrI*) and the crystallite size (*CrS*) were calculated following Nam (Eq. 1) and Scherrer (Eq. 2) equations, respectively [37–39].

$$CrI = \frac{A_{cr}}{A_{cr} + A_{am}} \tag{1}$$

$$CrS = \frac{K\lambda}{\beta_{1/2} cos 2\theta} \tag{2}$$

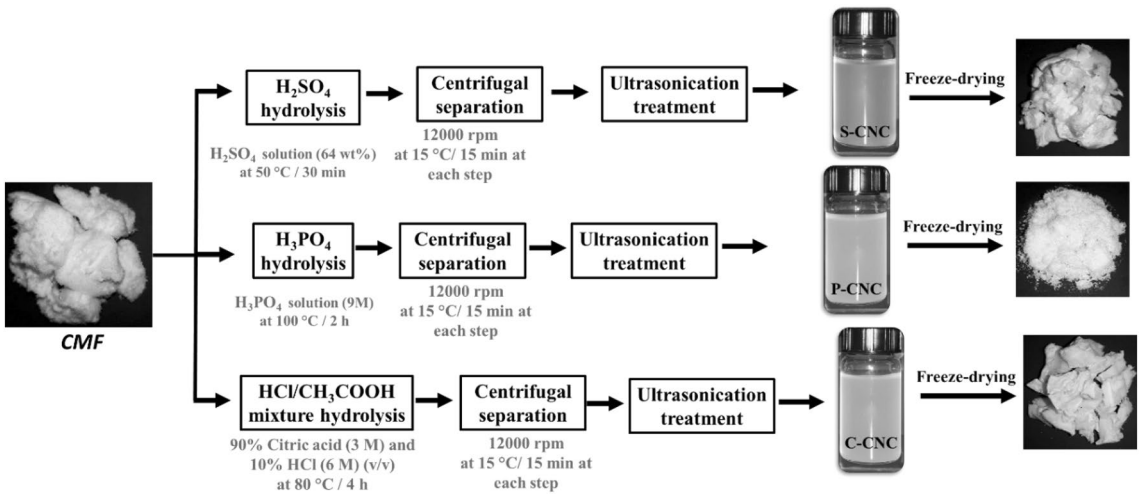

Fig. 2 Overall steps for the preparation of cellulose nanocrystals (S-CNC, P-CNC, and C-CNC)

where A_{cr} represents the area under the calculated pattern of crystalline cellulose. A_{am} is the area under the pattern calculated for the amorphous content. λ is the X-ray wavelength (λ = 1.5418 Å), *K* is the Scherrer constant (0.94), 2θ is the Bragg's angle (22°) and $\beta_{1/2}$ is the full width at the half maximum of the XRD peak. Scanning electron microscopy (HIROX SH 4000 M SEM apparatus) was used to observe the morphology of the samples. The SEM analysis was operated at an accelerating voltage of 15 kV. Samples were attached on SEM specimen holders with double-sided carbon tape and coated with carbon by using a high vacuum sputter coater. SEM images were statistically analyzed using ImageJ software to determine the diameter and length size of the samples. Atomic force microscopy (AFM) images of CNC were recorded using a Veeco Dimension ICON apparatus. The measurements were made at room temperature in tapping mode at a scan rate of 1.5 Hz. The thermal properties of all samples were also studied using thermogravimetry (Discovery TGA, TA instruments). The samples (≈ 10 mg) were heated from 30 to 700 °C, under nitrogen with an airflow of 25 mL/min and a heating rate of 10 °C/min.

Results and Discussions

Chemical Structure of Cellulosic Microfibers and Nanocrystals

Lignocellulosic materials are generally composed of cellulose, lignin, and hemicellulose, meaning that the fiber's main composition includes different functional groups such as aromatics, alcohols, alkanes, esters, carboxylates, and ketones [10, 40]. From the chemical composition results, it was found that R-AS contains 56% cellulose, 24% lignin, 1.29% moisture, and 3.12% ash. R-AS had a similar cellulosic composition to maize, hemp, and *Humulus japonicus* stems [33, 41, 42]. These findings suggest that R-AS could be used as an alternative to non-conventional cellulose sources [33].

FTIR analysis was performed to reveal the chemical structure changes that occurred after the alkaline, bleaching treatments and cellulose nanocrystals preparation. The FTIR spectra of R-AS, AT-AS, and CMF were obtained, as shown in Fig. 3a. The untreated raw *Artemisia annua* stem waste (R-AS) showed cellulose characteristic bands at 3334, 2919, and 1023 cm^{-1} corresponding to stretching vibrations of hydrogen bond O–H, C–H symmetrical stretching, and glycosidic ether band C–O–C, respectively [20, 33, 43]. The absorption band around 1636 cm^{-1} was assigned to the O–H bending of water [44]. The sharp peak at 1428 cm^{-1} can be attributed to C-H bending vibrations of cellulose [33]. Three peaks that are present only in the spectrum of R-AS at 1735 cm^{-1}, 1507 cm^{-1}, and 1234 cm^{-1}, which correspond respectively to C=O stretching vibration, C=C vibration of the aromatic skeleton, and C–O stretching vibration of acetyl or aryl functional groups from hemicellulose and lignin fractions [9, 45, 46]. These three bands practically disappear in the spectra of AT-AS and CMF after eliminating lignin and hemicelluloses after chemical treatments, which aligns with earlier reported studies in the literature [2, 20, 47]. Therefore, this confirms the stability of cellulose chemical structure and the total removal of lignin and hemicellulose molecules after chemical treatments [32].

The spectra of isolated CNC (Fig. 3b) revealed the same peaks in all wavenumbers like CMF spectra. However, the only difference is the intensity growth of cellulosic characteristics bands, indicating that the cellulose content was increased during different chemical treatments starting from R-AS and ending with extracted CNC. It has been reported that the use of sulfuric acid hydrolysis of cellulose induced a sulfate half-ester reaction between sulfuric acid and cellulose surface, which led to the occurrence of sulfate half-ester groups on the surface of CNC [6, 33]. On the other hand, phosphoric acid hydrolysis results in P-CNC with inserted phosphate groups on the surface [8]. While the carboxylate groups can be formed by the esterification reaction between the hydroxyl groups of cellulose and the carboxyl groups of citric acid, leading into carboxylated CNC (C-CNC) [7]. Hence, it is worth noting that sulfate and carboxylate groups were introduced on the surface of S-CNC, P-CNC, and C-CNC during the sulfuric, phosphoric and citric/hydrochloric acid hydrolysis, respectively. The band relative to sulfate and phosphate negatively charged groups is generally observed at 1202 and 1230 cm^{-1}, respectively, which are overlapped with the main characteristics of cellulose molecules in the FTIR spectrum of S-CNC, and P-CNC samples. In the case of C-CNC prepared using hydrochloric acid / citric acid mixture, a new peak at 1731 cm^{-1} was observed, due to the functionalization with the carboxylate groups through an esterification reaction between the O–H groups of cellulose and the COOH groups of citric acid [48]. The FTIR results confirmed the successful extraction of surface-functionalized CNC from the newly *Artemisia annua* stems. Overall, all typical absorption bands present in the isolated S-CNC, P-CNC, and C-CNC spectra are almost identical to the spectra of CNC obtained from tomato plant residue [1], hemp stalks [33], and sago seed shells [2].

Crystalline Structure of Cellulose Microfibers and Cellulose Nanocrystals

Cellulose commonly consists of both crystalline and amorphous regions [4, 49]; the crystalline structure of cellulose is due to hydrogen bonding interactions and Van der Waals forces between adjacent cellulosic monomers [19]. Identification of cellulosic materials types and evaluation

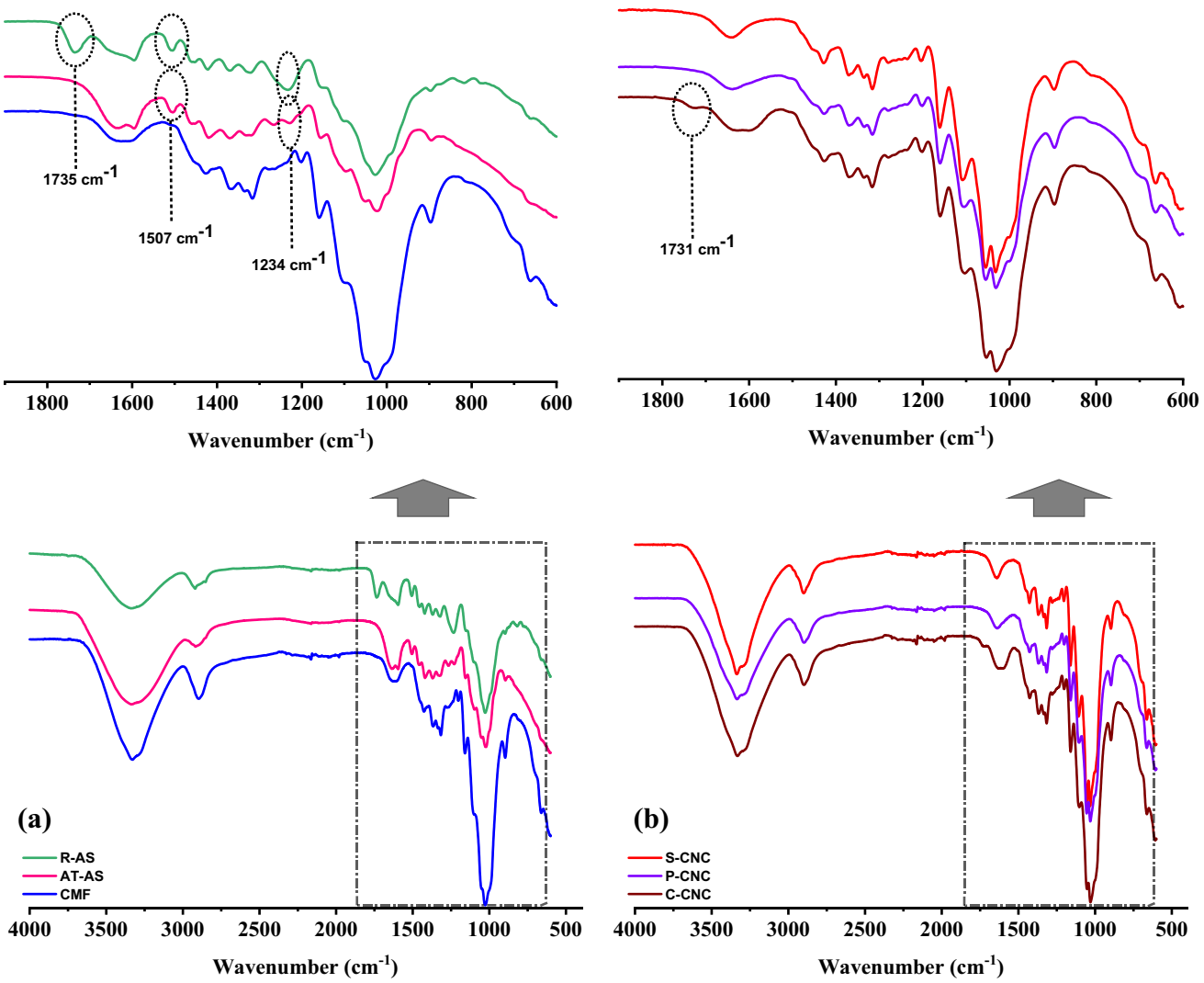

Fig. 3 FTIR spectra of **a** R-AS, AT-AS, and CMF; and **b** the isolated cellulose nanocrystals (S-CNC, P-CNC, C-CNC)

of crystallinity after different chemical treatment steps was determined using an X-ray diffractometer. Figure 4 presents the XRD spectra of R-AS, AT-AS, CMF, and all the obtained CNC after hydrolysis treatment (S-CNC, P-CNC, and C-CNC), whereas the value of *CrI* and *CrS* were summarized in Table 1. The R-AS and AT-AS exhibited three reflection peaks at 2θ = 16.1°, 22.3° and 34.5° (Fig. 4a), that are attributed to the crystal form of cellulosic polymorph. The R-AS sample displayed a broad peak at 2θ = 15–19°, which is attributed to the overlapping of crystalline cellulose I and the amorphous cellulose, hemicellulose, and lignin [50]. This result confirms that R-AS waste fibers can be classified as lignocellulosic material [1]. On the other hand, after obtaining CMF, intense crystalline peaks were observed at 2θ value of 17.4°, 22.9°, and 35.1°, confirming the cellulose crystalline structure and the successful removal of hemicellulose and lignin during chemical treatments.

During chemical hydrolysis, the acid attacks the amorphous parts of CMF and liberates individual crystallites via the initiation of glycosidic bonds hydrolytic cleavage, which instantly increases the crystallinity of cellulose [19]. The crystallinity index gradually increased from 57% for CMF to 84%, 79%, and 72% for S-CNC, P-CNC, and C-CNC, respectively (Table 1). These findings indicate the consecutive removal of the amorphous regions during acid hydrolysis. Furthermore, the highest crystallinity of isolated cellulose nanocrystals appeared in the presence of sulfuric acid, compared with the presence of phosphoric acid (P-CNC) and hydrochloric acid/citric acid mixture (C-CNC). This difference can be due to the easy penetration of sulfite ions in more accessible amorphous regions of CMF and disordered cellulosic regions were decomposed; hence, high crystallinity was obtained [19]. Moreover, the Bronsted acidity of the acids could have affected the crystallinity of CNC [51, 52].

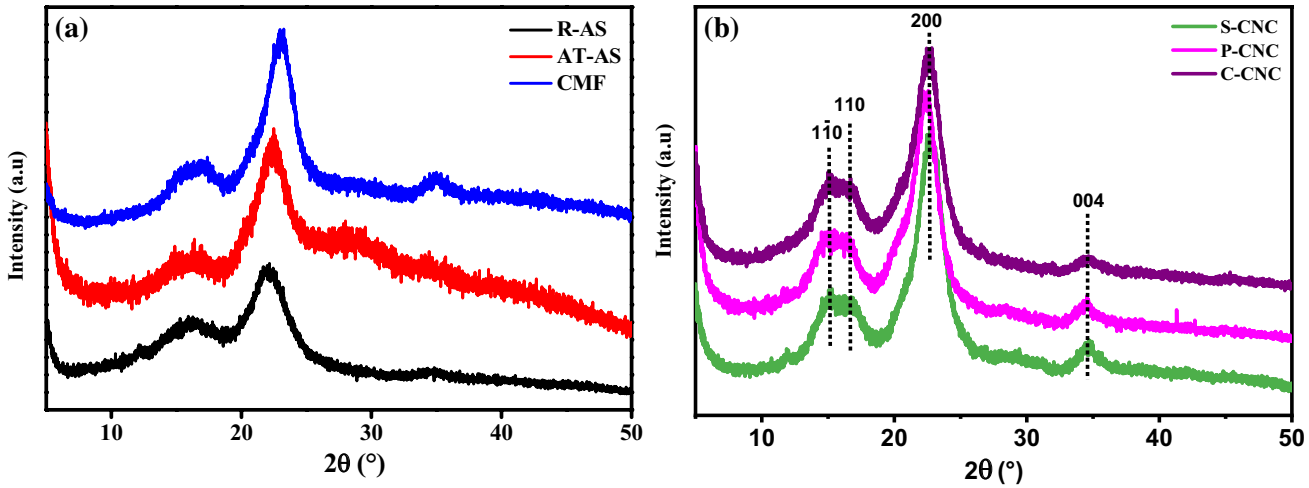

Fig. 4 XRD patterns of **a** R-AS, AT-AS, and CMF; and **b** the isolated cellulose nanocrystals (S-CNC, P-CNC, and C-CNC)

Table 1 Structural and thermal parameters of *S-CNC, P-CNC, and C-CNC samples*

Sample	*CrI* (%)	*CrS* (nm)	T_{onset} (°C)	T_{max} (°C)	*R* (%) at 700 °C
S-CNC	84	3.13	213	345	15.65
P-CNC	79	2.44	207	342	17.04
C-CNC	72	2.78	193	336	20.51

Accordingly, the average crystallites size (CrS) was determined from X-ray diffractograms by applying Scherrer's expression (Eq. 2). This calculation was made only for S-CNC, P-CNC, and C-CNC; based on which the CrS value was found to be 3.13, 2.44, and 2.78 nm, respectively. The CrS depend on the acid hydrolysis type and conditions. The high value of CrS for S-CNC is possibly due to rearrangement and recrystallizing of the purified α-cellulose chains from neighboring CMF during acid hydrolysis, leading to the generation of longer crystal dimensions and high crystallinity index of CNC.

Morphological Analysis of Raw and Treated Fibers

Morphological and microstructure were investigated from the original fibers to fibers exposed to various treatments because the source of cellulose and chemical treatment process has a profound influence on the dimension and properties. The SEM images of R-AS fibers as presented in Fig. 5a, showed an average width of 100–300 µm and a length is about 500 µm. However, the alkali-treated fibers (AT-AS) surface presents a non-uniform roughness due to the removal of the same amorphous compounds such as hemicellulose and lignin [44], and also the elimination of a large amount of the extractives molecules from the surface of the fibers (Fig. 5b). After bleaching treatment, the cellulosic fibers (Fig. 5c–d) were disintegrated into microfibers with a diameter between 5 and 30 µm. For the morphological aspect, the CMF appeared smoother than fibers found after alkali treatment (AT-AS), as more hemicellulose and lignin were removed during the bleaching process. This result shows that the applied chemical treatments effectively produced individual CMF from *Artemisia annua* plant stems.

Dimension and Aspect Ratio of Isolated CNC

The disintegration process of CMF to CNC depends on several parameters such as the concentration of acid, type of acid, temperature, and duration of the hydrolysis process [53]. Fragmentation of CMF starts with the cleavage of amorphous regions that are not resistant to acid hydrolysis and leaving crystalline regions. This leads to the isolation of nano-sized crystals of cellulose. In this study, the successful extraction of cellulose nanocrystals under acid hydrolysis conditions was confirmed by high-resolution AFM (Fig. 6). Referring to AFM results (Fig. 6), the nanocrystals tend to agglomerate due to the strong hydrogen bonds established between the individualized crystallites.

The obtained CNC exhibited a rod-shaped aspect, as generally observed for cellulose nanocrystals isolated using acid hydrolysis [2, 13]. By examining the AFM images (Fig. 6) using digital image analysis (Veeco Data Analysis software), the average diameter and length of the obtained CNC samples were calculated and reported (Table 2), which verified that the obtained CNC were on a nanometric scale. However, the diameter (*D*) and length (*L*) of the obtained S-CNC, P-CNC, and C-CNC showed some differences. The approximate diameters for cellulose nanocrystals under sulfuric acid, phosphoric acid,

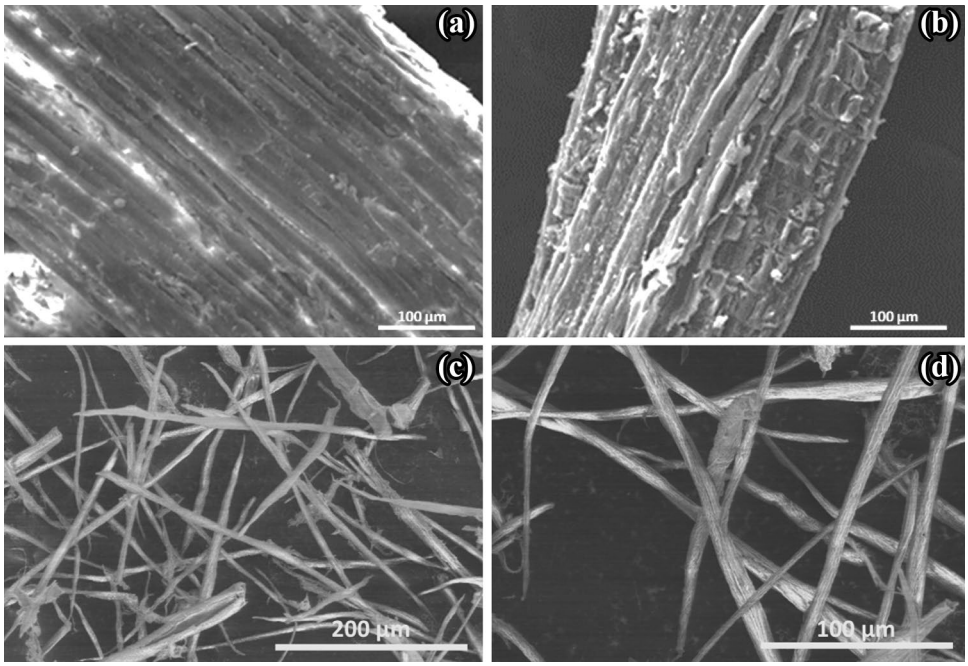

Fig. 5 SEM images of **a** R-AS fibers, **b** Alkali-treated fibers, **c** and **d** cellulose microfibers

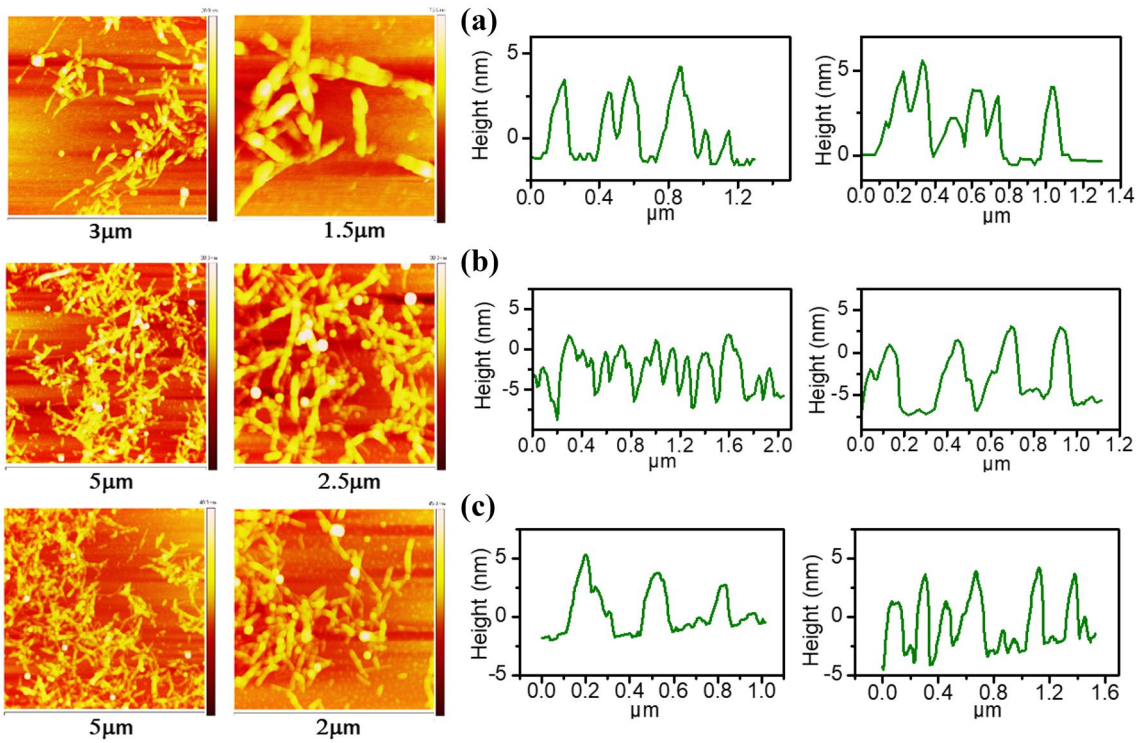

Fig. 6 AFM images and the corresponding height profiles taken along the indicated lines of **a** S-CNC, **b** P-CNC, and **c** C-CNC

and hydrochloric acid / citric acid mixture were found to be about 4.7, 5.3, and 7.2 nm, respectively. These results are close to those found for CNC isolated from tomato plant residue, garlic straw, eggplant plant, agave tequilana, barley, and pea pods (Table 2). Similarly, the average length values were found to be ranging from 380 to 520 nm. These results present an aspect ratio (*L/D*) of 81, 95, and 64 for S-CNC, P-CNC, and C-CNC, respectively.

Table 2 Length (*L*), diameter (*D*), aspect ratio (*L/D*), and hydrolysis process of cellulose nanocrystals isolated from different lignocellulosic sources

Source	*L* (nm)	*D* (nm)	*L/D*	Hydrolysis process	References
Tomato (*Solanum lycopersicum* L.) plant residue	367 ± 101	7.4 ± 2.2	49	H_2SO_4 (64wt%)	[1]
	670 ± 115	6.2 ± 2.4	98	H_3PO_4 (9 M)	
	514 ± 131	4.7 ± 1.4	67	Citric acid (6 M)/ HCl (3 M) mixture	
Garlic (*Allium sativum* L.) straw	480	6	80	H_2SO_4 (65wt%)	[19]
Eggplant (*Solanum melongena* L.) plant	487.0 ± 154	6.7 ± 2.1	74	H_2SO_4 (64wt%)	[9]
	597.5 ± 163	6.3 ± 2.3	89	H_3PO_4 (9 mol/L)	
Agave tequilana (*Agave L.*)	323 ± 113	11 ± 4	28	H_2SO_4 (65wt%)	[54]
Barley (*Hordeum vulgare* L.)	329 ± 123	10 ± 4	32	H_2SO_4 (65wt%)	
Pea (*Pisum Sativum* L.)	483 ± 74	5.4 ± 2.3	89	H_2SO_4 (64wt%)	[6]
Artemisia annua L	384 ± 93	4.7 ± 1.8	81	H_2SO_4 (64wt%)	This study
	504 ± 122	5.3 ± 1.2	95	H_3PO_4 (9 M)	
	456 ± 105	7.2 ± 2.1	64	Citric acid (3 M)/HCl (6 M) mixture	

Thermal Stability Behavior

The thermal degradation behavior of R-AS, CMF, and isolated cellulose nanocrystals (S-CNC, P-CNC, and C-CNC) was investigated by thermogravimetric analysis, which gives information about the degradation processes over time as the temperature change. Generally, the thermal degradation of lignocellulosic materials and its derivatives implicates dehydration, depolymerization, and glycosylic unit decomposition, followed by carbonaceous species formation [53]. The same thermal behavior was seen in this study, in which all the samples exhibited a weight loss below 5% at < 140 °C (Fig. 7), corresponding to the evaporation of moisture loosely bound to the surfaces, which is related to the hydrophilic nature of the cellulosic materials [6]. In the temperature between 150 and 700 °C (Fig. 7a and b), it can be seen that the R-AS sample showed two and three steps of the thermal degradation process under nitrogen and air atmosphere, respectively, which are well explained in the literature [6, 55, 56]. The first stage, occurring at 211 °C for both atmospheres, is assigned mainly due to the decomposition of hemicellulose to volatile compounds, which widely exist in biomass [57]. The intensive decomposition with major weight loss takes place in the second stage on DTG curves (Fig. 7a and b) at 345 °C, and 279 °C under nitrogen and air atmosphere, respectively, is due to the depolymerization, rearrangement, and pyrolysis, leading to the formation of CO, levoglucosan, and others volatile species by the cleavage of the main cellulosic chain, the abstraction of side groups and ring-opening reactions occur in this step [55, 57]. In this stage, it can be noticed that the main degradation DTG peak was shifted to a lower temperature under air atmosphere. The third step degradation between 365 and 455 °C under air atmosphere based on DTG curves (Fig. 7b), could be attributed to the degradation of lignin, and the oxidative decomposition of the charred residue. Since lignin is thermally more stable, its decomposition depends on the source and composition [56, 58]. As in the case of the nitrogen atmosphere (Fig. 7b), this peak is not detected. The combustion of carbonaceous species finally occurs at higher temperatures (> 460 °C), considering that the degradation of biomass rich in polysaccharides is accelerated by oxygen; its degradation is practically completed at about 500 °C. While in the nitrogen condition, the biochar was the dominant product. This result shows that R-AS contains heterogeneous constitute (hemicellulose, cellulose, and lignin).

After removing hemicellulose, lignin, and extractives during chemical treatment, the TGA analysis was performed for extracted CMF. From the TGA and DTG curves (Fig. 7a and b), the thermal degradation of CMF in both atmospheres, the first thermal event is due to break down of cellulosic components and the second event that occurs only in the air atmosphere is due to oxidation of the partially decomposed components. The CMF showed one main degradation peak temperature at around 342 °C under nitrogen atmosphere (Fig. 7a), which showed better thermal stability than the raw material (211 °C). This increase in thermal stability is due to increased crystallinity and intermolecular hydrogen-bonded domains after eliminating non-cellulosic and amorphous components [59]. In the air atmosphere (Fig. 7b), two weight loss stages, namely oxidative fast devolatilization at 320 °C and combustion stage at 418 °C, could be found. This degradation was mainly contributed by the oxygen in the air. The oxygen would accelerate the devolatilization by the combustion reaction with char. More importantly, the most significant difference between nitrogen and air atmosphere could be found in the third stage (combustion stage). This percentage of carbonaceous species of CMF under nitrogen atmosphere was 15 wt%. In the air atmosphere, almost all

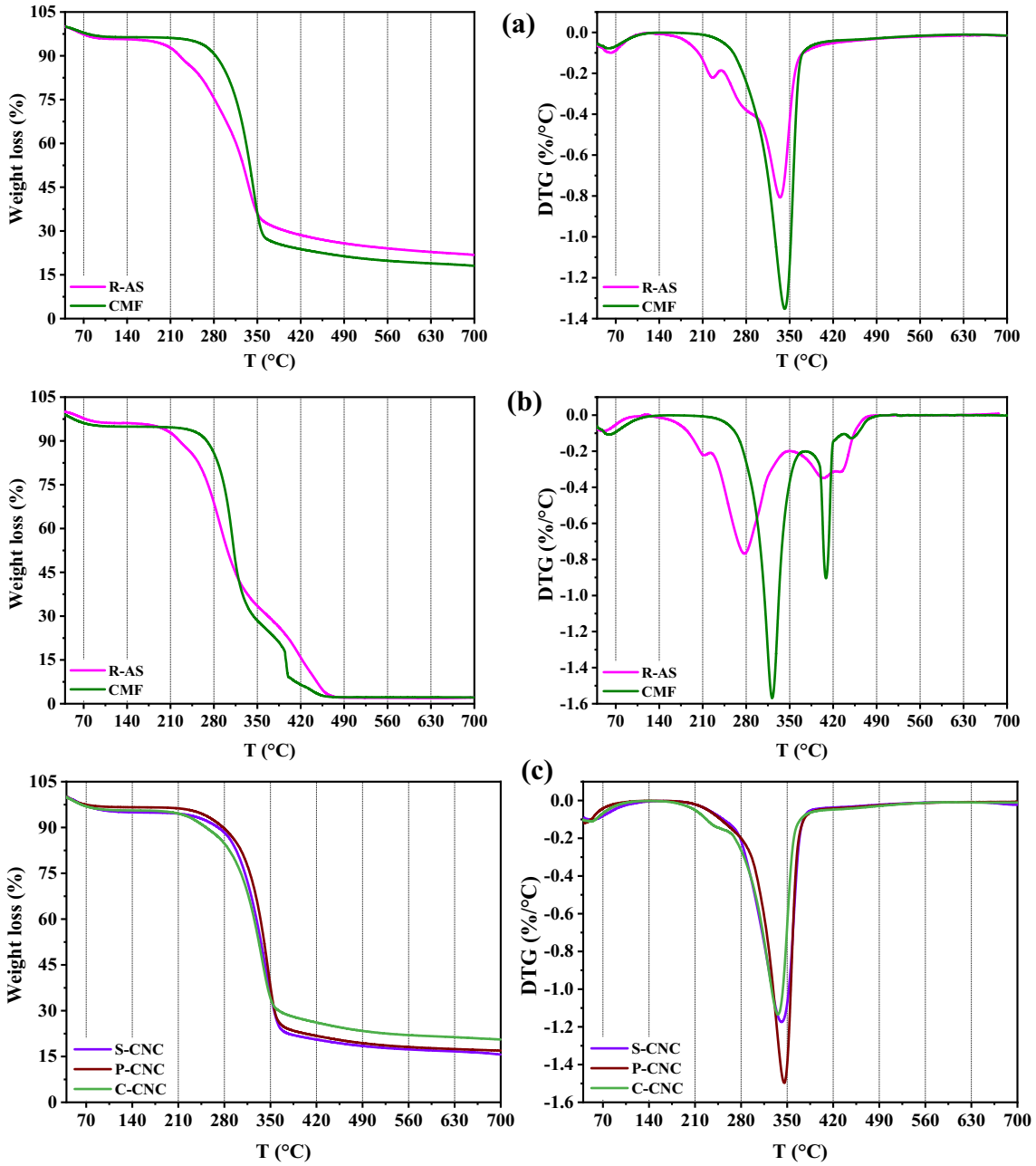

Fig. 7 TGA and DTG curves of R-AS and CMF samples under **a** nitrogen atmosphere and **b** air atmosphere, and of **c** S-CNC, P-CNC, and C-CNC samples under nitrogen atmosphere

the residual carbonaceous species formed in the oxidative fast devolatilization stage was burned with oxygen and converted into CO_2 and H_2O [15, 39].

Thermal decomposition of cellulose nanocrystals prepared under different acidic conditions results in one major peak in the high-temperature range of 335–346 °C in the DTG curve (Fig. 7c). It was observed that thermal degradation was initiated at 193 °C and 207 °C in the case of phosphoric acid and hydrochloric acid/citric acid mixture treatments, respectively. While the cellulose nanocrystals prepared using the sulfuric acid process was 213 °C. Comparing to both acid processed nanocrystals C-CNC and P-CNC, there was a significant increase in the initial degradation temperature of S-CNC (Table 1), which is higher than that extracted from other sources using sulfuric acid [19, 20]. A similar thermal property was noticed where microcrystalline cellulose extracted from giant reed using H_2SO_4 showed higher decomposition temperatures compared with different acid solutions [40]. These findings show that the different acid treatments produced CNC that have interesting

thermal properties. On the other hand, the residues left after heating to 700 °C were observed to be about 15.65, 17.04, and 20.51% for S-CNC, P-CNC, and C-CNC, respectively. The higher residual amounts produced by C-CNC are likely due to its functionalization during acid treatment [7].

Conclusion

This study was designed to prepare valuable cellulosic products from the residue of *Artemisia annua* stem waste, which was identified for the first time as a viable and sustainable materials source to produce cellulose microfibers and cellulose nanocrystals. Furthermore, a conventional extraction process based on alkali treatment followed by and bleaching was used to raw *Artemisia annua* stem waste. The non-cellulosic materials such as lignin and hemicellulose were used successfully removed. This process produced pure CMF with a diameter between 5 and 30 µm, with a T_{max} of 342 °C. The feasibility of CNC isolation was successfully carried out by exposing the extracted CMF to sulfuric, phosphoric, and hydrochloric/citric mixture acid hydrolysis, resulting in P-CNC, S-CNC, and C-CNC, respectively. The obtained CNC have high crystallinity, a uniform rod-shaped aspect with a size distribution of 4.7–7.2 nm in diameter and 384–504 nm in length, and improved thermal stability with T_{max} of 345, 342, and 336 °C for S-CNC, P-CNC, and C-CNC, respectively. Moreover, the crystallinity index was found to increase from 57% for CMF to 84, 79, and 72% for S-CNC, P-CNC, and C-CNC, respectively. Consequently, these findings demonstrate a potential strategy to add high value to *Artemisia annua* stem waste and proved that it could be used to produce valuable CMF and CNC, which may be used in various applications such as polymer reinforced composites manufacturing.

Acknowledgements The authors wish to acknowledge l'Office Chérifien des Phosphates (OCP S. A) for financial support.

Declarations

Conflict of interest The authors declare that they have no conflict of interest.

Ethical Approval The article does not include human participants and/or animals research.

Informed Consent Informed consent was obtained from all participants.

References

1. Kassab, Z., Kassem, I., Hannache, H., Bouhfid, R., Qaiss, A.E.K., El Achaby, M.: Tomato plant residue as new renewable source for cellulose production: extraction of cellulose nanocrystals with different surface functionalities. Cellulose **27**, 4287–4303 (2020). https://doi.org/10.1007/s10570-020-03097-7
2. Naduparambath, S., Jinitha, T.V., Shaniba, V., Sreejith, M.P., Balan, A.K., Purushothaman, E.: Isolation and characterisation of cellulose nanocrystals from sago seed shells. Carbohydr. Polym. **180**, 13–20 (2018). https://doi.org/10.1016/j.carbpol.2017.09.088
3. Taflick, T., Schwendler, L.A., Rosa, S.M.L., Bica, C.I.D., Nachtigall, S.M.B.: Cellulose nanocrystals from acacia bark–Influence of solvent extraction. Int. J. Biol. Macromol. **101**, 553–561 (2017). https://doi.org/10.1016/j.ijbiomac.2017.03.076
4. Rahman, N.H.A., Chieng, B.W., Ibrahim, N.A., Rahman, N.A.: Extraction and characterization of cellulose nanocrystals from tea leaf waste fibers. Polymers (Basel) **9**, 1–11 (2017). https://doi.org/10.3390/polym9110588
5. Trache, D., Thakur, V.K., Boukherroub, R.: Cellulose nanocrystals/graphene hybrids—a promising new class of materials for advanced applications, www.mdpi.com/journal/nanomaterials (2020)
6. Kassab, Z., Abdellaoui, Y., Salim, M.H., El Achaby, M.: Cellulosic materials from pea (Pisum Sativum) and broad beans (Vicia Faba) pods agro-industrial residues. Mater. Lett. **280**, 128539 (2020). https://doi.org/10.1016/j.matlet.2020.128539
7. Kassab, Z., Syafri, E., Tamraoui, Y., Hannache, H., Qaiss, A.E.K., El Achaby, M.: Characteristics of sulfated and carboxylated cellulose nanocrystals extracted from Juncus plant stems. Int. J. Biol. Macromol. **154**, 1419–1425 (2020). https://doi.org/10.1016/j.ijbiomac.2019.11.023
8. Ait Benhamou, A., Kassab, Z., Nadifiyine, M., Salim, M.H., Sehaqui, H., Moubarik, A., El Achaby, M.: Extraction, characterization and chemical functionalization of phosphorylated cellulose derivatives from Giant Reed Plant. Cellulose **28**, 4625–4642 (2021). https://doi.org/10.1007/S10570-021-03842-6
9. Bahloul, A., Kassab, Z., El Bouchti, M., Hannache, H., Qaiss, A.E.K., Oumam, M., El Achaby, M.: Micro- and nano-structures of cellulose from eggplant plant (*Solanum melongena* L.) agricultural residue. Carbohydr. Polym. **253**, 117311 (2021). https://doi.org/10.1016/J.CARBPOL.2020.117311
10. Ait Benhamou, A., Boussetta, A., Kassab, Z., Nadifiyine, M., Hamid Salim, M., Grimi, N., El Achaby, M., Moubarik, A.: Investigating the characteristics of cactus seeds by-product and their use as a new filler in phenol formaldehyde wood adhesive. Int. J. Adhes. Adhes. **110**, 102940 (2021). https://doi.org/10.1016/J.IJADHADH.2021.102940
11. Trache, D., Hussin, M.H., Haafiz, M., Thakur, V.K.: Recent progress in cellulose nanocrystals: sources and production. Nanoscale **9**, 17–25 (2017). https://doi.org/10.1039/c6nr09494e
12. Kassab, Z., Boujemaoui, A., Ben Youcef, H., Hajlane, A., Hannache, H., El Achaby, M.: Production of cellulose nanofibrils from alfa fibers and its nanoreinforcement potential in polymer nanocomposites. Cellulose **26**, 9567–9581 (2019). https://doi.org/10.1007/s10570-019-02767-5
13. Le Normand, M., Moriana, R., Ek, M.: Isolation and characterization of cellulose nanocrystals from spruce bark in a biorefinery perspective. Carbohydr. Polym. **111**, 979–987 (2014). https://doi.org/10.1016/j.carbpol.2014.04.092
14. Motaung, T.E., Linganiso, L.Z.: Critical review on agrowaste cellulose applications for biopolymers. Int. J. Plast. Technol. **22**, 185–216 (2018). https://doi.org/10.1007/s12588-018-9219-6
15. Eyley, S., Thielemans, W.: Surface modification of cellulose nanocrystals. Nanoscale **6**, 7764–7779 (2014). https://doi.org/10.1039/C4NR01756K
16. Thomas, B., Raj, M.C., B, A.K., H, R.M., Joy, J., Moores, A., Drisko, G.L., Sanchez, C.: Nanocellulose, a versatile green platform: from biosources to materials and their applications.

Chem. Rev. **118**, 11575–11625 (2018). https://doi.org/10.1021/ACS.CHEMREV.7B00627
17. Huang, S., Liu, X., Chang, C., Wang, Y.: Recent developments and prospective food-related applications of cellulose nanocrystals: a review. Cellulose **27**, 2991–3011 (2020). https://doi.org/10.1007/s10570-020-02984-3
18. Blilid, S., Katir, N., Haskouri, J.E., Lahcini, M., Royer, S., El Kadib, A.: Phosphorylated micro- vs. nano-cellulose: a comparative study on their surface functionalisation, growth of titanium-oxo-phosphate clusters and removal of chemical pollutants. New J. Chem. **43**, 15555–15562 (2019). https://doi.org/10.1039/C9NJ03187A
19. Kallel, F., Bettaieb, F., Khiari, R., García, A., Bras, J., Chaabouni, S.E.: Isolation and structural characterization of cellulose nanocrystals extracted from garlic straw residues. Ind. Crops Prod. **87**, 287–296 (2016). https://doi.org/10.1016/j.indcrop.2016.04.060
20. Larissa, L.A., Fonsêca, A.F., Pereira, F.V., Druzian, J.I.: Extraction and characterization of cellulose nanocrystals from corn stover. Cellul. Chem. Technol. **49**, 127–133 (2015)
21. Trache, D.: Nanocellulose as a promising sustainable material for biomedical applications. AIMS Mater. Sci. **5**, 201 (2018)
22. Wallaart, T.E., Pras, N., Beekman, A.C., Quax, W.J.: Seasonal variation of artemisinin and its biosynthetic precursors in plants of *Artemisia annua* of different geographical origin: proof for the existence of chemotypes. Planta Med. **66**, 57–62 (2000). https://doi.org/10.1055/s-2000-11115
23. Aftab, T., Khan, M.M.A., Idrees, M., Naeem, M., Singh, M., Ram, M.: Stimulation of crop productivity, photosynthesis and artemisinin production in *Artemisia annua* L. by triacontanol and gibberellic acid application. J. Plant Interact. **5**, 273–281 (2010). https://doi.org/10.1080/17429141003647137
24. Liu, K.C.-S., Yang, S., Roberts, M.F., Elford, B.C., Phillipson, J.D.: Antimalarial activity of *Artemisia annua* flavonoids from whole plants and cell cultures. Plant Cell Rep. **11**, 11–14 (1992). https://doi.org/10.1007/BF00236389
25. Haq, F.U., Roman, M., Ahmad, K., Rahman, S.U., Shah, S.M.A., Suleman, N., Ullah, S., Ahmad, I., Ullah, W.: *Artemisia annua*: trials are needed for COVID-19. Phyther. Res. (2020). https://doi.org/10.1002/ptr.6733
26. Larson, H.J.: A call to arms: helping family, friends and communities navigate the COVID-19 infodemic. Nat. Rev. Immunol. **20**, 449–450 (2020). https://doi.org/10.1038/s41577-020-0380-8
27. Syukur, M., Lestari, E.G., Purnamaningsih, R., Yunita, R., Aisyah, S.I., Firdaus, R.: Adaptability of mutant genotypes of artemisia (*Artemisia annua* L.) as result of gamma irradiation in three locations. **33**, 251–257 (2011)
28. Tu, Y.: Studies on the Cultivation and Breeding of *Artemisia annua* L. from *Artemisia annua* L. to Artemisinins, pp. 139–161 (2017). https://doi.org/10.1016/b978-0-12-811655-5.00007-6
29. World Health Organization: WHO monograph on good agricultural and collection practices (GACP) for *Artemisia annua* L, pp. 1–49. WHO Press (2006)
30. Pakharenko, V., Sameni, J., Konar, S., Pervaiz, M., Yang, W., Tjong, J., Oksman, K., Sain, M.: Cellulose nanofiber thin-films as transparent and durable flexible substrates for electronic devices. Mater. Des. **197**, 109274 (2020). https://doi.org/10.1016/j.matdes.2020.109274
31. Blilid, S., Kędzierska, M., Miłowska, K., Wrońska, N., Achaby, M.E., Katir, N., Belamie, E., Alonso, B., Lisowska, K., Lahcini, M., Bryszewska, M., Kadib, A.E.: Phosphorylated micro- and nanocellulose-filled chitosan nanocomposites as fully sustainable, biologically active bioplastics. ACS Sustain. Chem. Eng. **8**, 18354–18365 (2020). https://doi.org/10.1021/ACSSUSCHEMENG.0C04426
32. El Achaby, M., Kassab, Z., Aboulkas, A., Gaillard, C., Barakat, A.: Reuse of red algae waste for the production of cellulose nanocrystals and its application in polymer nanocomposites. Int. J. Biol. Macromol. **106**, 681–691 (2018). https://doi.org/10.1016/j.ijbiomac.2017.08.067
33. Kassab, Z., Abdellaoui, Y., Salim, M.H., Bouhfid, R., Qaiss, A.E.K., El Achaby, M.: Micro- and nano-celluloses derived from hemp stalks and their effect as polymer reinforcing materials. Carbohydr. Polym. **245**, 116506 (2020). https://doi.org/10.1016/j.carbpol.2020.116506
34. Kassab, Z., Aziz, F., Hannache, H., Ben Youcef, H., El Achaby, M.: Improved mechanical properties of k-carrageenan-based nanocomposite films reinforced with cellulose nanocrystals. Int. J. Biol. Macromol. **123**, 1248–1256 (2019). https://doi.org/10.1016/j.ijbiomac.2018.12.030
35. Kassem, I., Ablouh, E.-H., Bouchtaoui, F.-Z., Kassab, Z., Khouloud, M., Sehaqui, H., Ghalfi, H., Alami, J., Achaby, M.E.L.: Cellulose nanocrystals-filled poly (vinyl alcohol) nanocomposites as waterborne coating materials of NPK fertilizer with slow release and water retention properties. Int. J. Biol. Macromol. (2021). https://doi.org/10.1016/j.ijbiomac.2021.08.093
36. Jonasson, S., Bünder, A., Niittylä, T., Oksman, K.: Isolation and characterization of cellulose nanofibers from aspen wood using derivatizing and non-derivatizing pretreatments. Cellulose **27**, 185–203 (2019). https://doi.org/10.1007/S10570-019-02754-W
37. Shaheen, T.I., Emam, H.E.: Sono-chemical synthesis of cellulose nanocrystals from wood sawdust using acid hydrolysis. Int. J. Biol. Macromol. **107**, 1599–1606 (2018). https://doi.org/10.1016/j.ijbiomac.2017.10.028
38. Nam, S., French, A.D., Condon, B.D., Concha, M.: Segal crystallinity index revisited by the simulation of X-ray diffraction patterns of cotton cellulose Iβ and cellulose II. Carbohydr. Polym. **135**, 1–9 (2016). https://doi.org/10.1016/J.CARBPOL.2015.08.035
39. Ling, Z., Wang, T., Makarem, M., Santiago Cintrón, M., Cheng, H.N., Kang, X., Bacher, M., Potthast, A., Rosenau, T., King, H., Delhom, C.D., Nam, S., Vincent Edwards, J., Kim, S.H., Xu, F., French, A.D.: Effects of ball milling on the structure of cotton cellulose. Cellulose **26**, 305–328 (2019). https://doi.org/10.1007/S10570-018-02230-X
40. Tarchoun, A.F., Trache, D., Klapötke, T.M., Derradji, M., Bessa, W.: Ecofriendly isolation and characterization of microcrystalline cellulose from giant reed using various acidic media. Cellulose **26**, 7635–7651 (2019). https://doi.org/10.1007/s10570-019-02672-x
41. Jiang, Y., Zhou, J., Zhang, Q., Zhao, G., Heng, L., Chen, D., Liu, D.: Preparation of cellulose nanocrystals from Humulus japonicus stem and the influence of high temperature pretreatment. Carbohydr. Polym. **164**, 284–293 (2017). https://doi.org/10.1016/J.CARBPOL.2017.02.021
42. Longaresi, R.H., de Menezes, A.J., Pereira-da-Silva, M.A., Baron, D., Mathias, S.L.: The maize stem as a potential source of cellulose nanocrystal: cellulose characterization from its phenological growth stage dependence. Ind. Crops Prod. **133**, 232–240 (2019). https://doi.org/10.1016/J.INDCROP.2019.02.046
43. Naili, H., Jelidi, A., Limam, O., Khiari, R.: Extraction process optimization of Juncus plant fibers for its use in a green composite. Ind. Crops Prod. **107**, 172–183 (2017). https://doi.org/10.1016/J.INDCROP.2017.05.006
44. Kumar, A., Negi, Y.S., Choudhary, V., Bhardwaj, N.K.: Characterization of cellulose nanocrystals produced by acid-hydrolysis from sugarcane bagasse as agro-waste. J. Mater. Phys. Chem. **2**, 1–8 (2014). https://doi.org/10.12691/jmpc-2-1-1
45. Kumar, A., Negi, Y.S., Bhardwaj, N.K., Choudhary, V.: Synthesis and characterization of cellulose nanocrystals/PVA based bionanocomposite. Adv. Mater. Lett. **4**, 626–631 (2013). https://doi.org/10.5185/amlett.2012.12482

46. Chieng, B.W., Lee, S.H., Ibrahim, N.A., Then, Y.Y., Loo, Y.Y.: Isolation and characterization of cellulose nanocrystals from oil palm mesocarp fiber. Polymers (Basel) **9**, 1–11 (2017). https://doi.org/10.3390/polym9080355
47. Tarchoun, A.F., Trache, D., Klapötke, T.M.: Microcrystalline cellulose from Posidonia oceanica brown algae: extraction and characterization. Int. J. Biol. Macromol. **138**, 837–845 (2019). https://doi.org/10.1016/j.ijbiomac.2019.07.176
48. Yu, H.Y., Zhang, D.Z., Lu, F.F., Yao, J.: New approach for single-step extraction of carboxylated cellulose nanocrystals for their use as adsorbents and flocculants. ACS Sustain. Chem. Eng. **4**, 2632–2643 (2016). https://doi.org/10.1021/acssuschemeng.6b00126
49. El Omari, H., Ablouh, E., Brouillette, F., Taourirte, M., Belfkira, A.: New method for determining paper surface energy per contact angle. Cellulose **26**, 9295–9309 (2019). https://doi.org/10.1007/s10570-019-02695-4
50. Jiang, F., Hsieh, Y.-L.: Cellulose nanocrystal isolation from tomato peels and assembled nanofibers. Carbohydr. Polym. **122**, 60–68 (2015). https://doi.org/10.1016/j.carbpol.2014.12.064
51. Kadib, A.E., Finiels, A., Brunel, D.: Sulfonic acid functionalised ordered mesoporous materials as catalysts for fine chemical synthesis. Chem. Commun. **49**, 9073–9076 (2013). https://doi.org/10.1039/C3CC45160G
52. Chen, S.S., Yu, I.K.M., Tsang, D.C.W., Yip, A.C.K., Khan, E., Wang, L., Ok, Y.S., Poon, C.S.: Valorization of cellulosic food waste into levulinic acid catalyzed by heterogeneous Brønsted acids: Temperature and solvent effects. Chem. Eng. J. **327**, 328–335 (2017). https://doi.org/10.1016/J.CEJ.2017.06.108
53. George, J., Ramana, K.V., Bawa, A.S.: Bacterial cellulose nanocrystals exhibiting high thermal stability and their polymer nanocomposites. Int. J. Biol. Macromol. **48**, 50–57 (2011). https://doi.org/10.1016/j.ijbiomac.2010.09.013
54. Espino, E., Cakir, M., Domenek, S., Román-Gutiérrez, A.D., Belgacem, N., Bras, J.: Isolation and characterization of cellulose nanocrystals from industrial by-products of Agave tequilana and barley. Ind. Crops Prod. **62**, 552–559 (2014). https://doi.org/10.1016/j.indcrop.2014.09.017
55. Jiang, J., Li, J., Hu, J., Fan, D.: Effect of nitrogen phosphorus flame retardants on thermal degradation of wood. Constr. Build. Mater. **24**, 2633–2637 (2010). https://doi.org/10.1016/j.conbuildmat.2010.04.064
56. Gebke, S., Thümmler, K., Sonnier, R., Tech, S., Wagenführ, A., Fischer, S.: Flame retardancy of wood fiber materials using phosphorus-modified wheat starch. Molecules **25**, 335 (2020). https://doi.org/10.3390/molecules25020335
57. Liu, C., Wang, H., Karim, A.M., Sun, J., Wang, Y.: Catalytic fast pyrolysis of lignocellulosic biomass. Chem. Soc. Rev. **43**, 7594–7623 (2014). https://doi.org/10.1039/C3CS60414D
58. Liao, J.J., Latif, N.H.A., Trache, D., Brosse, N., Hussin, M.H.: Current advancement on the isolation, characterization and application of lignin (2020)
59. Antal, M.J., Várhegyi, G., Jakab, E.: Cellulose pyrolysis kinetics: revisited. Ind. Eng. Chem. Res. **37**, 1267–1275 (1998). https://doi.org/10.1021/ie970144v